Metals & corrosion

Quasi in situ investigation on the influence of particle stimulate nucleation on recrystallization textures in TiB$_2$ particles reinforced Al-3wt%Mg composites

Y. D. Chen[1], C. Y. Dan[1,*] (iD), C. Chen[2], C. X. Chen[2], L. Jin[1,3], H. W. Wang[1], and Z. Chen[1,*]

[1] *State Key Laboratory of Metal Matrix Composites, Shanghai Jiao Tong University, Shanghai 200240, People's Republic of China*
[2] *Beijing Key Laboratory of Civil Aircraft Structures and Composite Materials, COMAC Beijing Aircraft Technology Research Institute, Beijing 102211, China*
[3] *China Nuclear Power Design Co., Ltd, Shenzhen 518100, People's Republic of China*

ABSTRACT

Particle-reinforced metal matrix composites generally have different recrystallized textures compared with unreinforced alloys. During annealing, the large local strain in the particle deformation zone (PDZ) induces particle stimulated nucleation (PSN) of recrystallized grains, influencing the final recrystallized texture. Quasi in situ EBSD observation was conducted in a TiB$_2$/Al-3wt%Mg composite to study the PSN behavior around clustered TiB$_2$ particles. PSN grains were found to recrystallize faster and related to the local strain in the PDZs. However, compared with grains recrystallized from other sites, the PSN grains still could not grow out of the PDZs. Thus, orientation preference in the grain growth process, known as oriented growth, influenced a little on the textures of all PSN grains. According to the statistics of orientations of recrystallized grains around TiB$_2$ particles, PSN grains tended to randomize recrystallized textures.

Introduction

During annealing, recrystallization and following grain growth occurred in deformed alloys can change the grain structures and textures, which relate to the properties of alloy. Accordingly, thermal mechanical process is a common method to obtain desired properties. For example, bimodal grains can form after designed annealing [1] or partial recrystallization [2, 3] to enhance the ductility of alloys. Goss textures can be generated by utilizing abnormal grain growth to improve the magnetic properties of silicon steel [4–6]. As a critical issue, well-designed grain structures or textures need a solid understanding of the contributing factors for recrystallization.

With the addition of particles, particle-reinforced metal matrix composites can possess enhanced mechanical properties, and thus be widely used in activation and automotive fields [7, 8]. However, the recrystallization behavior of composites during annealing always differs from that of alloys due to the presence of particles [9, 10]. The influences of particles on recrystallization are twofold. On the one hand, particles may retard recrystallization by preventing the migration of grain boundaries, known as Zener pinning [11]. On the other hand, particles may also promote the formation of new recrystallized grains via particle-stimulated nucleation (PSN) [12, 13]. Since particles' deformability are generally smaller than the matrix, severe local deformation will present in the regions adjutant to particles, known as the particle deformation zones (PDZs) [14, 15]. In PDZs, a high density of dislocations is stored and rapid recovery as well as formation of recrystallized nuclei is possible upon annealing.

Besides accelerating the recrystallization, PSN was also reported to influence the recrystallization textures. Many previous studies related the formation of P-orientation grains to the PSN phenomenon [16–19]. However, after verification by Tangen [16] and Engler [20], it was found that the formation of P texture was attributed not only to PSN but also to the oriented growth of recrystallized grains. In other words, the P-oriented nuclei become a dominant texture in the final recrystallized state because they grow faster than grains of other orientations. Therefore, the strengthening of P texture is not an inevitable consequence of PSN. A number of researchers believed that PSN would actually weaken the recrystallized texture and randomize the orientation distribution [21–23]. On the basis of acknowledging oriented growth, Lücke [24] calculated the recrystallized texture of PSN, and it was found that the final recrystallized texture tended to be random. Recently, various research on the thermomechanical treatments of Al-based alloys and composites also discovered that when influenced by PSN, the textures tended to be random [25–27].

The controversy of the topic stems from some intrinsic difficulties that can hardly be resolved in these previous studies. Textures in completely recrystallized polycrystalline alloys resulted from various nucleation sites, like deformation bands, grain boundaries, and so on [15]. Thus, comparing the recrystallized textures of the alloy with and without particles could not isolate the influence of PSN from other nucleation sites. By inferring the process from those observed results, this method was also poor at accurately verifying the influence of oriented growth on PSN orientations, because the orientation relationships between grains would change during the grain growth process [5, 28]. Besides, if PSN originates from particles whose dissolution or precipitation behavior is temperature-dependent, influence of PSN on recrystallization textures can be disrupted by protean pinning force [29–31]. In polycrystalline alloy, in situ experiments enabling the observation of the whole recrystallization process can be used to study the changes of orientations caused by PSN properly.

Quasi in situ recrystallization experiments of TiB_2/Al–Mg composites were conducted to investigate the orientations of PSN grains. Because of the thermal stability of TiB_2 particles [32, 33], no dissolution or precipitation behavior could interfere with the observation of PSN behavior. The process from deformation state to recrystallized grain growth was tracked, with which the factors affecting PSN orientations were also discussed.

Materials and methods

Al-3wt%Mg alloy and two TiB_2-reinforced composites with the same Mg content but varying TiB_2 particles fraction, 1wt%TiB_2/Al-3wt%Mg and 5wt%TiB_2/Al-3wt%Mg, were prepared in State Key Laboratory of Metal Matrix Composites, Shanghai Jiao Tong University. The composites were fabricated by in situ mixed salt method [34–36]. Blocks of alloys and composites were cold-rolled with a 70% reduction in the normal rolling direction (ND). Specimens with 10 mm in the rolling direction (RD) and 8 mm in the transverse direction (TD) were cut from the as-deformed sheets. A Tescan MAIA3 scanning electron microscope (SEM) equipped with an Electron-backscattered diffraction (EBSD) detector Bruker e-FlashHR was used for EBSD characterization. For EBSD detection, the RD-ND section of specimens was first mechanically polished and then polished with 0.04 μm SiO_2 solution for 60 min. The quasi in situ annealing experiment was conducted at 300 °C on Al-3wt%Mg-1wt%TiB_2 with the SEM and a peripheral furnace. To track the same zone after annealing, several indentations were marked on the polished

surface with 1 N force for 15 s. In order to avoid the influence of indentations on the recrystallizations, the chosen area for observation were away from the indentation marks. After observing the as-rolled state in SEM, the sample was taken out and placed in a furnace, which had already been heated to 300 °C. The sample was repositioned into the electron microscope, and the same area could continue to be observed with the location of the indention marks. Transmission electron microscopy (TEM) samples at as-deformed state were prepared through mechanical polishing and final thinning using a twin-jet polishing unit with a solution containing 30% methanol and 70% nitric acid at 0 °C. TEM examinations were carried out using Talos F200X.

Results

Deformed microstructures

The microstructures of the studied materials after rolling are summarized in Fig. 1. The grains of unreinforced Al-3%Mg alloy were elongated along the RD with a large number of shear bands inside. After deformation, the most strained regions with the highest dislocation density were those inside the shear bands and close to grain boundaries (especially triple junctions), with a lower EBSD detection rate due to severe lattice distortion. After heating at high temperatures, these regions could be the potential nucleation sites for recrystallization.

On the other hand, for deformed composites containing TiB_2 particles, shear bands resembling those in unreinforced Al-3%Mg alloy were barely detected (Fig. 1b and c). The regions bearing most of the strain during deformation were now PDZs around TiB_2 particles. In the prepared composites, some TiB_2 particles agglomerated to form clusters. Small amounts of these particle clusters were located within the grains, while most were at grain boundaries, as shown in Fig. 1b and c. When the content of TiB_2 particles increased from 1 to 5wt%, more particle clusters were detected on the ND-RD section. In metallic materials containing particles, these particle clusters were easy to accumulate dislocations during deformation, resulting in the formation of PDZs around particles [14]. Therefore, for TiB_2-reinforced Al–Mg composites, PDZs around clustered particles

would act as an important recrystallization nucleation site.

The deformed textures of the unreinforced alloy and reinforced composite are compared in Fig. 1d. For unreinforced Al–Mg alloy, the texture was dominated by deformed texture components including Copper $\{112\}<111>$ (27.1%), Brass $\{110\}<112>$ (15.9%) and S $\{123\}<634>$ (14.3%), while fractions of recrystallized textures like Cube $\{001\}<100>$, P $\{011\}<122>$ and Goss $\{011\}<100>$ were much smaller. The fraction of Goss was only 4.0% and almost no Cube and P were detected in Al–Mg alloy after the rolling. Different from unreinforced alloy, the fractions of those texture components in composites were relatively uniform. For example, with 5wt% TiB_2 particles addition, although Copper was still the texture component with the highest fraction, its fraction decreased to 10.1%. The fractions of S and Brass decreased to 3.5% and 5.3%, respectively. The fractions of Goss and P were 5.1% and 1.9%. With a fraction smaller than 1%, Cube was still rare in composites after rolling.

Orientation in PDZs

Misorientations between PDZ around particles and matrix away from particles have been observed by previous researchers [16, 37]. As shown in the region in Fig. 2a, a severely deformed zone around particles existed. According to the IPF mapping, the orientation of the regions (in color blue) close to the severely deformed zone differed from the orientation of the matrix (in color green). As the {111} PF of the entire region in Fig. 2c, orientation of the deformed grain rotated around the axis close to the TD direction. After annealing, recovery mainly happened in severely deformed zone. This previously difficult-to-detect zone was gradually able to be detected by EBSD as in Fig. 2b. Orientation of part recovered region labeled with a red point in Fig. 2b is plotted in PF of Fig. 2c. Orientation of this recovered region was similar to those of regions (in color blue) close to severely deformed zone before annealing. Misorientation compared with the recovered region with red point along the white line in Fig. 2b started from red point, and the result is shown in Fig. 2d. The continuous orientation development along the white line indicated the misorientations existed between PDZs and the matrix of deformed grain.
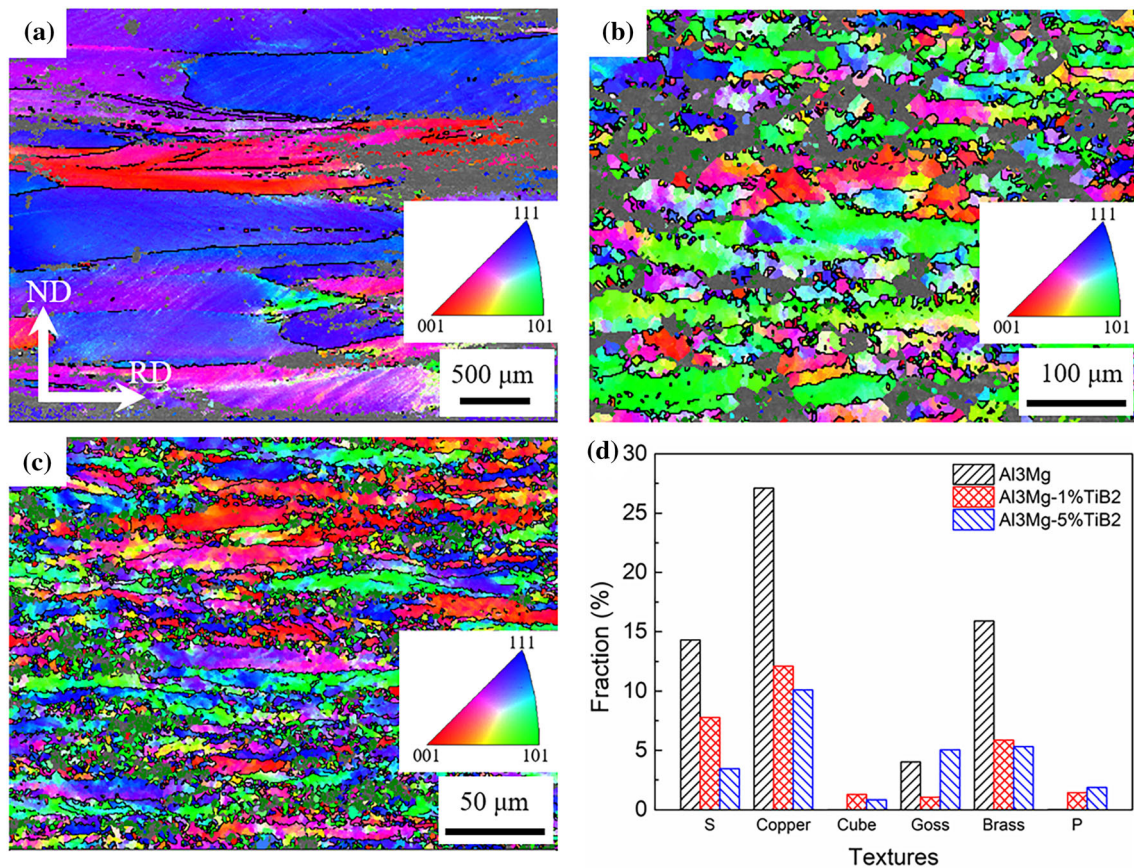
Figure 1 Microstructure of different Al–Mg alloys and composites. **a–c** show ND-RD sections of Al-3%Mg, 1%TiB$_2$/Al-3%Mg and 5%TiB$_2$/Al-3%Mg after rolling. The fraction of texture components in these materials are summarized in **d**. Green phases in **b** and **c** are TiB$_2$ particles.

Quasi in situ *observation on the PSN around TiB$_2$ clusters*

With the addition of TiB$_2$ particles, the change of recrystallization nucleation sites was related to the increase in PDZs and the decrease in shear bands. Besides, because of the smaller grain size in the composites compared with the unreinforced alloy as in Fig. 1, area of grain boundaries in composites was also larger than that in the alloy. Thus, the number of potential recrystallization nucleation at grain boundaries in unreinforced alloy and reinforced composites were also different. If the recrystallized textures of polycrystalline composites after annealing is directly compared with those of unreinforced alloy, the differences in textures should be influenced by various nucleation sites. Thus, to obtain the sole influence of PSN on orientations, in situ observation of the PDZs is necessary.

In the region shown in Fig. 3a, some TiB$_2$ particles were present inside grains and some were on grain boundaries. Here we focused on the TiB$_2$ particle clusters found inside a specific grain (labeled as D1) and at grain boundaries between D1 and three other grains (labeled as D2, D3 and D4). Severely deformed zone existed after rolling were marked with a dotted blue line in Fig. 3a and shown in Fig. 3b and c with higher magnification. Those area were difficult to detect by EBSD due to the high strain localization. For regions close to the particle clusters but could be detected by EBSD, they underwent an orientation change compared with those away from the particle clusters according to the color of IPF map. There were many low angle grain boundaries (gray lines) or even some high angle grain boundaries (black lines) in regions close to particles as in Fig. 3. With the influences of TiB$_2$ particles and their neighboring grains, the orientations of grains D1-D4 after rolling were
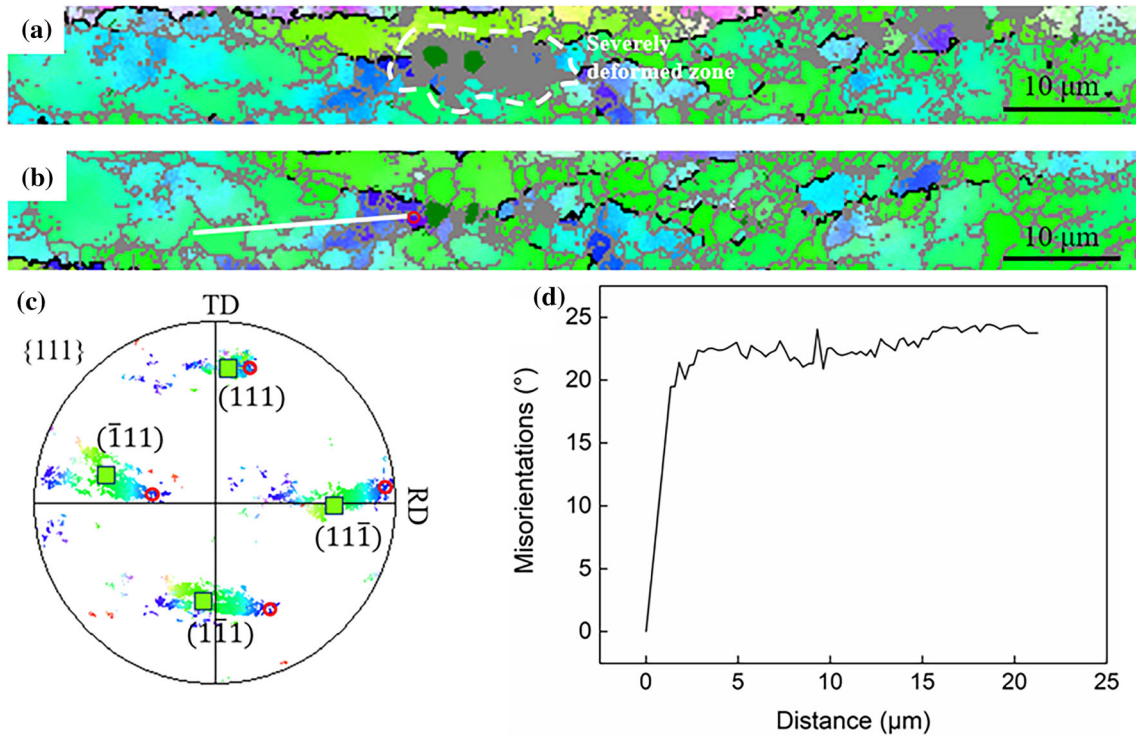
Figure 2 Misorientations between PDZs and region away from particles. **a** and **b** show the evolution inside a grain before and after annealing at 300 °C for 5 min. **c** is the PF showing the orientation relationship between the red point in **b** and the matrix of the grain. **d** shows misorientation along the white line in **b** compared with the orientation of the red point. The phases in color green are TiB$_2$ particles.

complicated. The {111} Pole figures (PFs) of grain D1-D4 are shown as Fig. 3d–f, correspondingly. The distributions of the orientations of the four grains on the PFs were scattered, indicating a certain rotation inside these grains during the deformation. The rotation axes of those grains were all close to TD.

After annealing at 300 °C for 5 min, as shown in Fig. 4a, recrystallized grains or nuclei formed in severely deformed regions which were difficult to detect at as-rolled state (Fig. 3a–c). A new recrystallized grain R1 nucleated at the lower right corner of TiB$_2$ in grain D1 (Fig. 4b). The orientation relationship between recrystallized grain R1 and deformed grain D1 is shown in PF in Fig. 4d. The orientation of PSN grain R1 rotated by $16°$ around $<0\bar{1}2>$ from matrix of grain D1. The other three recrystallized grains, R2, R3 and R4 formed around TiB$_2$ at the grain boundary intersection of four deformed grains D1-D4 (Fig. 4c). The orientations of R2, R3 and R4 were plotted in the PFs with orientations of deformed grains D1-D4 as shown in Fig. 4e–h, correspondingly. From those four PFs, three recrystallized grains R2-

R4 were not similar to any orientation of four surrounding deformed grains. The orientation relationship between these three recrystallized grains R2-R4 and the surrounding four deformed grains D1-D4 is calculated and shown in Table 1. Misorientations between recrystallized grains and deformed grains were all different, while three recrystallized grains R2-R4 all had small misorientation angles with one of their neighboring deformed grains. For example, the misorientation between R2 and its neighboring deformed grain D1 was $21°$, smaller than misorientations between R2 and D2-D4.

After further annealing the sample for another 20 min, there were some other grains recrystallized in the focused region as shown in Fig. 5. Many of those new recrystallized grains were larger than the PSN grains R1-R4, while PSN grains still kept almost the same size and morphology when comparing Fig. 4a. Even when the sample has fully recrystallized, as in Fig. 5b and c, recrystallized grains around clustered TiB$_2$ particles were still smaller than those away from TiB$_2$ particles.
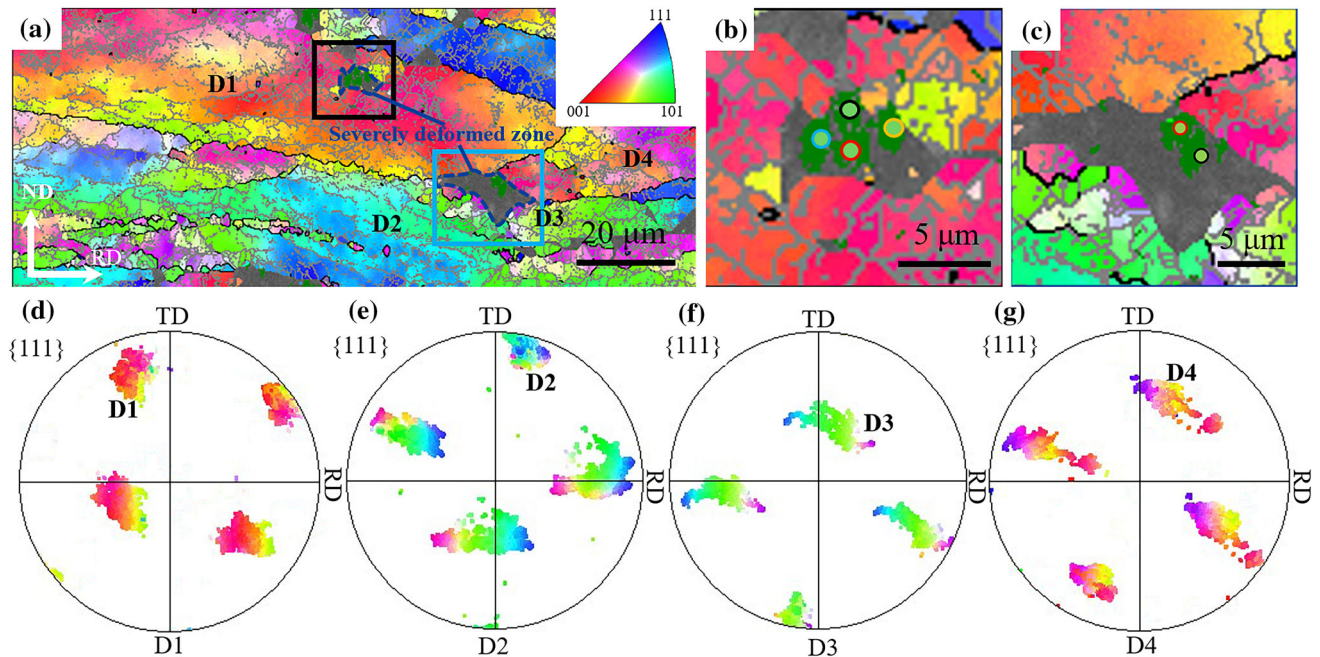
Figure 3 A region shows both particle clusters inside grain and on grain boundaries prior to annealing. **a** shows there are severely deformed zones around the particle clusters. **b** shows the particle clusters and surrounding PDZ inside grain D1, which is a graph with higher magnification in black rectangle in **a**. **c** shows the particle clusters and surrounding PDZ on grain boundary junctions of grain D1-D4, which is a graph with higher magnification in light blue rectangle in **a**. **d**–**g** are {111} PFs showing the orientations of grain D1-D4. TiB$_2$ particles are in the green phase and the clustered ones in **b** and **c** are marked with points.
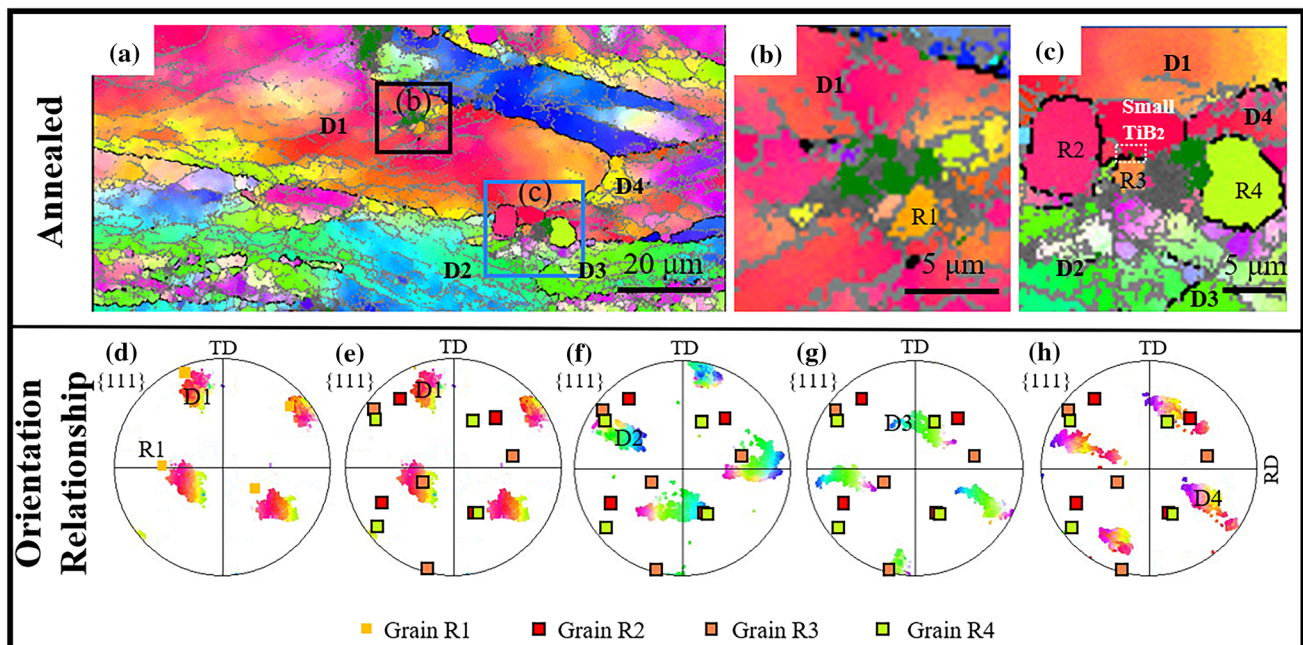

Figure 4 PSN occurred around TiB$_2$ particles inside a grain and on grain boundaries after annealing. **a**–**c** show the microstructure after annealing at 300 °C for 5 min in the same zone of Fig. 3. **d**–**h** are {111} PFs representing orientation relationships between PSN grains and deformed grains. **d** compares orientations of grain R1 and deformed grain D1. **e**–**h** compare orientations of grain R2-R4 and deformed grain D1-D4, correspondingly.

Table 1 Orientation relationships between recrystallized grain R2-R4 and deformed grain D1-D4, respectively

Misorientations	R2	R3	R4
D1	$21°\langle 124\rangle$	$40°\langle \overline{3}4\overline{3}\rangle$	$49°\langle \overline{2}1\overline{4}\rangle$
D2	$45°\langle 1\overline{3}3\rangle$	$21°\langle 130\rangle$	$57°\langle 21\overline{2}\rangle$
D3	$53°\langle \overline{2}43\rangle$	$30°\langle 432\rangle$	$48°\langle \overline{1}21\rangle$
D4	$51°\langle \overline{2}33\rangle$	$24°\langle 1\overline{4}1\rangle$	$28°\langle \overline{2}34\rangle$

Discussion

Origin of PSN orientations

As the results in "Orientation in PDZs" section, misorientation had already existed between orientations inside PDZs and those of neighboring deformed grains. The results in "Quasi in situ observation on the PSN around TiB2 clusters" section also indicated that there were obvious rotations between the PSN grains and the neighboring deformed grains. In the traditional understanding of the origin of recrystallized texture, the orientations of recrystallized grains are inherited from deformed orientations [38, 39]. Accordingly, after annealing, newly recrystallized PSN grains had orientations inherited from PDZs and

then inherited the misorientations between PDZ and neighboring deformed grains.

Thus, the orientation of PSN grains before further grain growth could be determined by two factors: (1) the orientation of deformed grains that form PDZs around the particles; (2) misorientations between PSN grains and deformed grains inherited from those between PDZs and deformed grains. Within TiB2-reinforced Al–Mg composites, the orientations of deformed grains are usually randomly distributed because there are lacking of strongly deformed textures when compared with alloy as shown in Fig. 1d. Thus, the orientations of neighboring deformed grains are more possible to be different for different sites of PSN. As for the misorientation angle between PDZ and matrix, it is related to the amount of local strain accumulated in PDZ [40], which is in turn influenced by particle size. As shown in Fig. 6, microstructures around two TiB2 particles with different sizes were different. TiB2 particle in Fig. 6a was about 1 μm, larger than another particle in Fig. 6b with size of about 600 nm. The local dislocation densities in the zone around large particle were higher than that around the small one. Influenced by these dislocations, the lattice around the particles rotated and generated misorientation with the matrix

Figure 5 PSN grains in Al-3%Mg-1%TiB$_2$ composites are difficult to grow after further annealing. **a** show the partially recrystallized microstructures in the same zone of Figs. 3 and 4, after annealing at 300 °C for 25 min. **b** and **c** are part of zones in composites after full recrystallization. The phases in color green are TiB$_2$ particles.
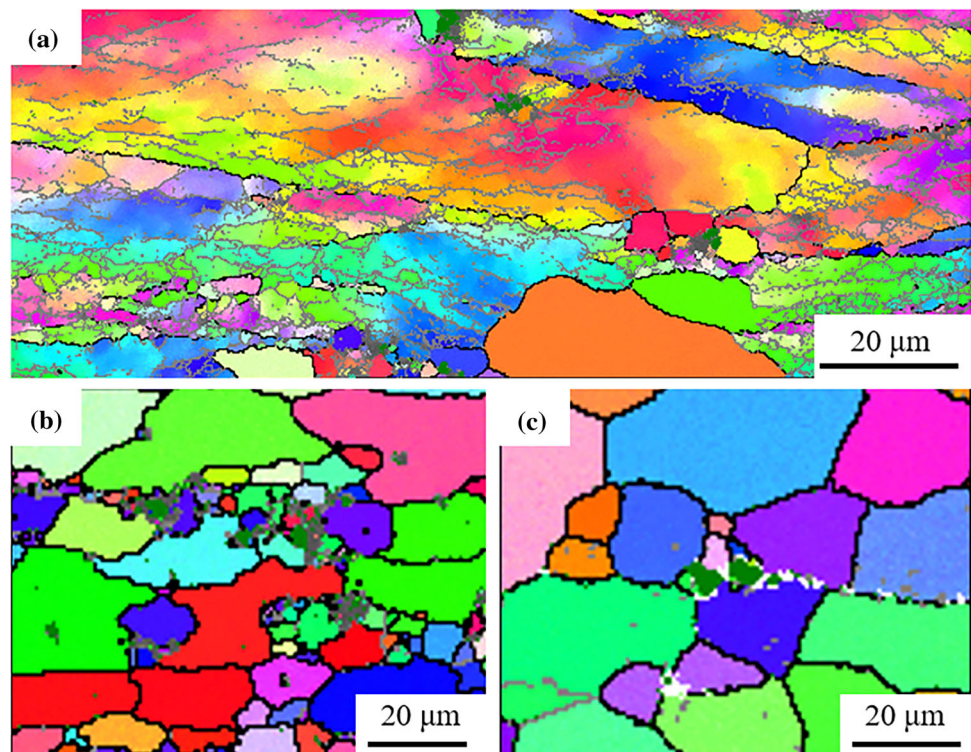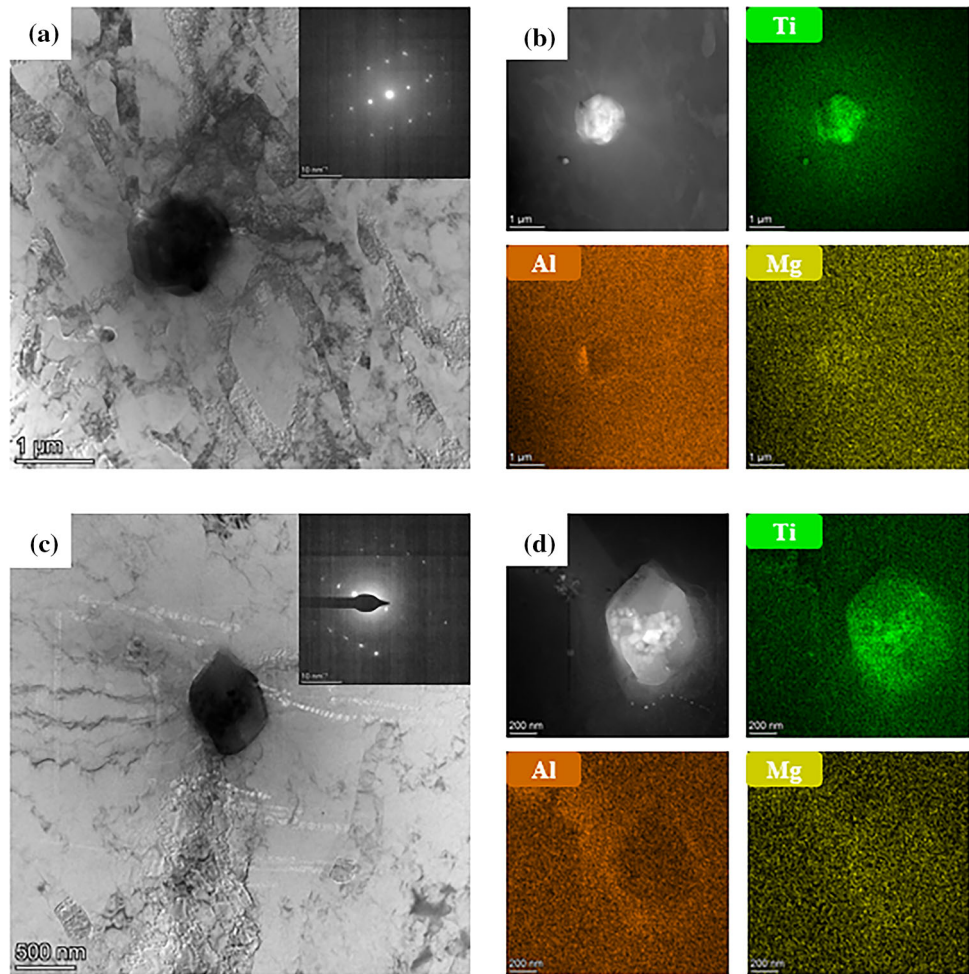
Figure 6 Bright field of TEM showing the dislocation densities around TiB$_2$ particles with different sizes. **a** and **c** are two TiB$_2$ particles which can be proved by the EDS in **b** and **d**. TiB$_2$ particle in **a** is larger than that in **c**.

away from particles. Because the size of particles and particle clusters are also different from this research and some previous studies [32, 41], the local strain in different PDZs is also different. Influenced by those two factors, different orientations of deformed grains and different local strains, the PSN grains from different PDZs are more possible to have different orientations.

Influence of grain growth on PSN orientations

Grain growth behavior of recrystallized grains after nucleation could also affect texture development. Based on the grain growth theory, the migration rate of grain boundary during the recrystallization stage can be expressed as [42, 43]:

$$V = MP_{eff} \tag{1}$$

where M is the mobility of grain boundaries, P_{eff} is the effective driving force for grain growth.

Therefore, the texture development during grain growth process is mainly controlled by the mobility of the grain boundary and the driving force acting on grain boundaries. In previous studies, the strengthening of textures by PSN was commonly related to oriented growth rather than the nucleation process of PSN [16, 20, 44]. Generally, these previous studies found that some orientations from PSN could grow faster than others, which may result from high mobility (M) grain boundaries with $40\overset{\circ}{} < 111 >$ orientation relationship. It has been observed that certain orientations from PSN retain growth advantages even when Zener pinning force of the second-phase particles reduces the effective driving force P_{eff} [29, 45, 46]. Therefore, the grain growth process can affect the overall orientations if PSN grains are capable of growing during the subsequent annealing. However, in the TiB$_2$-reinforced Al–Mg composites, it was found to be difficult for PSN grains to grow upon further annealing as in Fig. 5. This suggests that
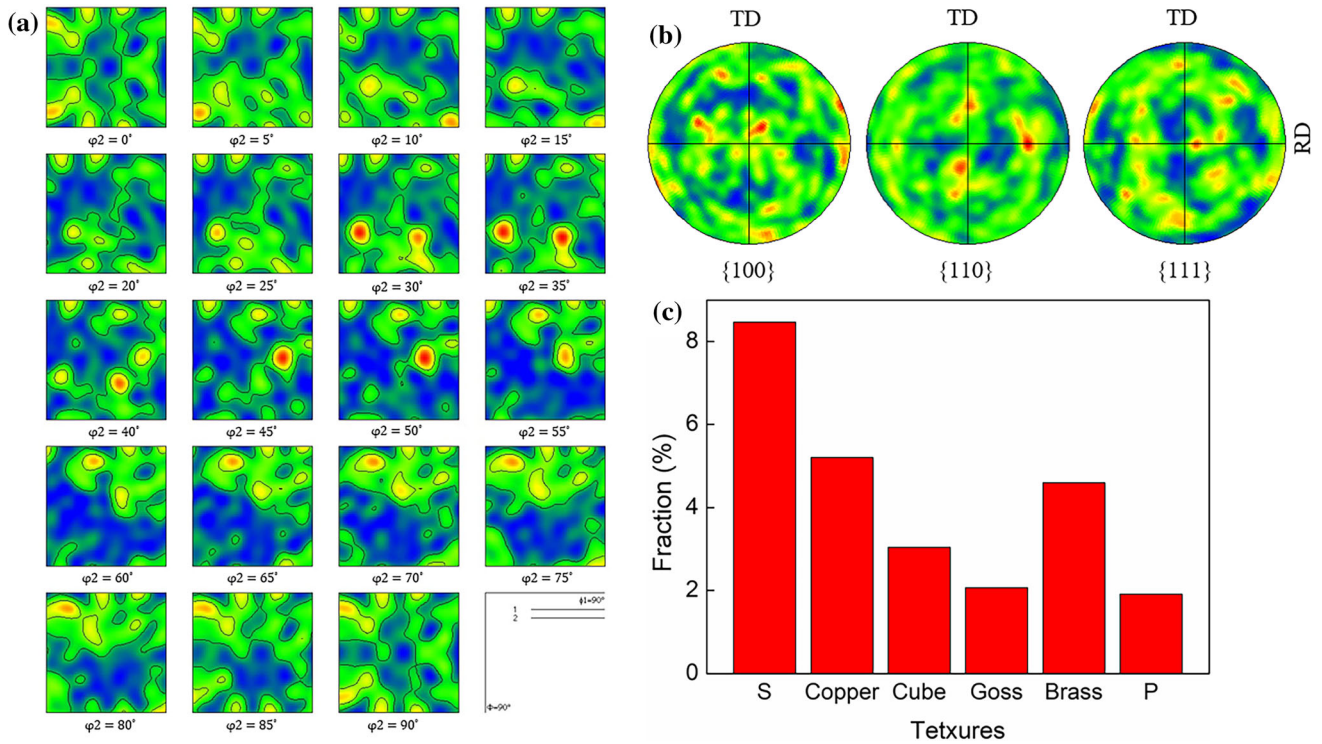
Figure 7 Textures of recrystallized grains around TiB$_2$ particles in Al-3wt%Mg-1wt%TiB$_2$. **a** is ODF maps and **b** is PFs showing the textures are random. **c** shows fractions of different textures.

PSN grains do not have a growth advantage over other recrystallized grains. Two possible reasons for this phenomenon are that PSN grains may not have the high-mobility grain boundary of $40° < 111 >$-type orientation relationship with their neighboring deformed grains (such is the case of grain R1, R2 and R4), or their growth may be completely retarded by Zener pinning of the particles (particularly nanosized particles, which often present in the composites). It is well-acknowledged that it would be more difficult to grow when recrystallized grains impinge on each other. As a result, those PSN grains around clustered TiB$_2$ particles cannot grow to large size after exhausting the PDZs. The growth of PSN grains is unlikely to affect the final recrystallization texture in any significant manner and it should be difficult for the orientations of PSN grains to produce strong textures in TiB$_2$-reinforced Al–Mg composites.

To verify this, the orientation of recrystallized grains around TiB$_2$ particles in the Al-3wt%Mg-1wt%TiB$_2$ composite is concluded in Fig. 7. Because most of the recrystallized grains around TiB$_2$ particles should recrystallize from PDZs, this result could to

some extent reflect the influence of PSN on the recrystallization textures. From the orientation distribution function (ODF) of Fig. 7a and the PF of Fig. 7b, the orientations of the recrystallized grains around TiB$_2$ were relatively random, and only a slightly stronger S texture existed. As in Fig. 7c, the fraction of S-oriented grains was about 8.5% and the fractions of other typical texture components were basically no larger than 5.0%. Most of the rest were randomly oriented grains. It should be particularly noted that P orientation, which was often associated with the PSN phenomenon in some previous studies [16–19], was weak in recrystallized grains around TiB$_2$ particles as shown in Fig. 7c. This is because the fraction of Copper orientation, which can form $40° < 111 >$ grain boundaries with P orientations [16], in composites was smaller than alloys as shown in Fig. 1. Besides, influenced by Zener pinning force of TiB$_2$ particles on grain boundaries, those P-oriented grains also cannot grow up. Thus, it is reasonable that PSN grains induced by TiB$_2$ particle clusters were difficult to produce a strong P texture. In conclusion, PSN grains recrystallized around clustered TiB$_2$

particles tend to randomize the final recrystallization textures.

Conclusions

This work investigated the recrystallization and textures caused by PSN in TiB_2 particles reinforced Al-3wt%Mg composites. With quasi in situ experiments, the same zone containing PDZs around TiB_2 particles before and after recrystallization was tracked, and the individual contribution of PSN to recrystallized texture was studied. The following conclusions have been drawn from this work.

(1) Obvious misorientation existed between the PSN grains and the neighboring deformed grains. The misorientations inherited from those between PDZs and deformed grains were determined by local strain in PDZs, which is related to the size of TiB_2 particles.

(2) During further annealing, PSN grains could hardly grow out of PDZs resulting from the pinning effects of particles and misorientations. Because the grain growth behavior had little effect on the PSN grains, the oriented growth could not influence PSN orientations.

(3) Due to the relatively random deformed textures in composite and different local strain in PDZs affected by different TiB_2 particle sizes, PSN orientations tended to randomize textures, which was consistent with the statistical results.

Author contributions

YDC contributed to conceptualization, investigation, and writing—original draft. CYD contributed to writing—review and editing, formal analysis, and methodology. CC contributed to project administration and data curation. CXC contributed to visualization. LJ contributed to resources and validation. HWW contributed to funding acquisition. ZC contributed to supervision.

Data and code availability

Some or all data that support the findings of this study are available from the corresponding author upon reasonable request.

Declarations

Conflict of interest   The authors declare no conflict of interest.

References

[1] Wang Y, Chen M, Zhou F, Ma E (2002) High tensile ductility in a nanostructured metal. Nature 419:912–915. https://doi.org/10.1038/nature01133

[2] Wu X, Yang M, Yuan F, Wu G, Wei Y, Huang X, Zhu Y (2015) Heterogeneous lamella structure unites ultrafine-grain strength with coarse-grain ductility. Proc Natl Acad Sci 112(47):14501–14505. https://doi.org/10.1073/pnas.1517193112

[3] Wu SW, Wang G, Wang Q, Jia YD, Yi J, Zhai QJ, Liu JB, Sun BA, Chu HJ, Shen J, Liaw PK, Liu CT, Zhang TY (2019) Enhancement of strength-ductility trade-off in a high-entropy alloy through a heterogeneous structure. Acta Mater 165:444–458. https://doi.org/10.1016/j.actamat.2018.12.012

[4] Hayakawa Y, Muraki M, Szpunar J (1998) The changes of grain boundary character distribution during the secondary recrystallization of electrical steel. Acta Mater 46(3):1063–1073. https://doi.org/10.1016/S1359-6454(97)00303-0

[5] Shimizu R, Harase J, Dingley D (1990) Prediction of secondary recrystallization texture in Fe-3% Si by three-dimensional texture analysis. Acta Metall Mater 38(6):973–978. https://doi.org/10.1016/0956-7151(90)90169-H

[6] Homma H, Hutchinson B (2003) Orientation dependence of secondary recrystallisation in silicon–iron. Acta Mater 51(13):3795–3805. https://doi.org/10.1016/s1359-6454(03)00193-9

[7] Ibrahim I, Mohamed F, Lavernia E (1991) Particulate reinforced metal matrix composites—a review. J Mater Sci 26(5):1137–1156. https://doi.org/10.1007/BF00544448

[8] Wang M, Chen D, Chen Z, Wu Y, Wang F, Ma N, Wang H (2014) Mechanical properties of in-situ TiB2/A356

composites. Mater Sci Eng A 590:246–254. https://doi.org/10.1016/j.msea.2013.10.021

[9] Chen Z, Sun GA, Wu Y, Mathon MH, Borbely A, Chen D, Ji G, Wang ML, Zhong SY, Wang HW (2017) Multi-scale study of microstructure evolution in hot extruded nano-sized TiB₂ particle reinforced aluminum composites. Mater Des 116:577–590. https://doi.org/10.1016/j.matdes.2016.12.070

[10] Ramesh C, Keshavamurthy R, Koppad PG, Kashyap K (2013) Role of particle stimulated nucleation in recrystallization of hot extruded Al 6061/SiCp composites. Trans Nonferr Metal Soc 23(1):53–58. https://doi.org/10.1016/S1003-6326(13)62428-0

[11] Smith CS (1948) Grains, phases, and interfaces: an introduction of microstructure. Trans Metall Soc AIME 175:15–51

[12] Konrad J, Zaefferer S, Raabe D (2006) Investigation of orientation gradients around a hard laves particle in a warm-rolled Fe₃Al-based alloy using a 3D EBSD-FIB technique. Acta Mater 54(5):1369–1380. https://doi.org/10.1016/j.actamat.2005.11.015

[13] Xu W, Ferry M, Cairney J, Humphreys F (2007) Three-dimensional investigation of particle-stimulated nucleation in a nickel alloy. Acta Mater 55(15):5157–5167. https://doi.org/10.1016/j.actamat.2007.05.045

[14] Humphreys FJ (1997) A unified theory of recovery, recrystallization and grain growth, based on the stability and growth of cellular microstructures—II. The effect of second-phase particles. Acta Mater 45(12):5031–5039. https://doi.org/10.1016/S1359-6454(97)00173-0

[15] Humphreys FJ, Hatherly M (2004) Recrystallization and related annealing phenomena, 2nd edn. Elsevier, Oxford

[16] Tangen S, Sjølstad K, Furu T, Nes E (2010) Effect of concurrent precipitation on recrystallization and evolution of the P-texture component in a commercial Al-Mn alloy. Metall Mater Trans A 41(11):2970–2983. https://doi.org/10.1007/2Fs11661-010-0265-8

[17] Zang Q, Yu H, Lee Y-S, Kim M-S, Kim H-W (2018) Hot deformation behavior and microstructure evolution of annealed Al-7.9 Zn-2.7 Mg-2.0 Cu (wt%) alloy. J Alloys Compd 763:25–33. https://doi.org/10.1016/j.jallcom.2018.05.307

[18] Wang X, Guo M, Zhang J, Zhuang L (2016) Effect of Zn addition on the microstructure, texture evolution and mechanical properties of Al–Mg–Si–Cu alloys. Mater Sci Eng A 677:522–533. https://doi.org/10.1016/j.msea.2016.09.084

[19] Zang Q, Yu H, Lee Y-S, Kim M-S, Kim H-W (2019) Effects of initial microstructure on hot deformation behavior of Al-7.9 Zn-2.7 Mg-2.0 Cu (wt%) alloy. Mater Charact 151:404–413. https://doi.org/10.1016/j.matchar.2019.03.019

[20] Engler O, Hirsch J, Lücke K (1995) Texture development in Al-1.8 wt% Cu depending on the precipitation state—II. Recrystallization textures. Acta Metall Mater 43(1):121–138. https://doi.org/10.1016/0956-7151(95)90268-6

[21] Engler O, Yang P, Kong X (1996) On the formation of recrystallization textures in binary Al-1.3% Mn investigated by means of local texture analysis. Acta Mater 44(8):3349–3369. https://doi.org/10.1016/1359-6454(95)00416-5

[22] Humphreys FJ (2000) Particle stimulated nucleation of recrystallization at silica particles in nickel. Scr Mater 43(7):591–596. https://doi.org/10.1016/S1359-6462(00)00442-5

[23] Borkar H, Pekguleryuz M (2013) Microstructure and texture evolution in Mg–1% Mn–Sr alloys during extrusion. J Mater Sci 48(4):1436–1447. https://doi.org/10.1007/s10853-012-6896-y

[24] Engler O, Lücke K (1992) Mechanisms of recrystallization texture formation in aluminium alloys. Scr Metall Mater 27(11):1527–1532. https://doi.org/10.1016/0956-716X(92)90139-6

[25] She H, Shu D, Dong A, Wang J, Sun B, Lai H (2019) Relationship of particle stimulated nucleation, recrystallization and mechanical properties responding to Fe and Si contents in hot-extruded 7055 aluminum alloys. J Mater Sci Technol 35(11):2570–2581. https://doi.org/10.1016/j.jmst.2019.07.014

[26] Jain VKS, Yazar K, Muthukumaran S (2019) Development and characterization of Al5083-CNTs/SiC composites via friction stir processing. J Alloys Compd 798:82–92. https://doi.org/10.1016/j.jallcom.2019.05.232

[27] Adam KF, Long Z, Field DP (2017) Analysis of particle-stimulated nucleation (PSN)-dominated recrystallization for hot-rolled 7050 aluminum alloy. Metall Mater Trans A 48(4):2062–2076. https://doi.org/10.1007/s11661-017-3967-3

[28] Song HY, Liu HT, Jonas JJ, Wang GD (2017) Effect of primary recrystallization microstructure on abnormal growth of goss grains in a twin-roll cast grain-oriented electrical steel. Mater Des 131:167–176. https://doi.org/10.1016/j.matdes.2017.06.016

[29] Huang K, Li Y, Marthinsen K (2015) Effect of heterogeneously distributed pre-existing dispersoids on the recrystallization behavior of a cold-rolled Al–Mn–Fe–Si alloy. Mater Charact 102:92–97. https://doi.org/10.1016/j.matchar.2015.02.015

[30] Ånes HW, van Helvoort AT, Marthinsen K (2023) Orientation dependent pinning of (sub) grains by dispersoids during recovery and recrystallization in an Al–Mn alloy. Acta Mater 248:118761. https://doi.org/10.1016/j.actamat.2023.118761

[31] Moghanaki SK, Kazeminezhad M, Logé R (2017) Effect of concurrent precipitation on the texture evolution during continuous heating of multi directionally forged solution treated Al–Cu–Mg alloy. Mater Charact 131:399–405. https://doi.org/10.1016/j.matchar.2017.07.033

[32] Dan C, Chen Z, Ji G, Zhong S, Wu Y, Brisset F, Wang H, Ji V (2017) Microstructure study of cold rolling nanosized in-situ TiB2 particle reinforced Al composites. Mater Des 130:357–365. https://doi.org/10.1016/j.matdes.2017.05.076

[33] Hamdad N, Benosman N, Bouhafs B (2010) First principles calculation of electronic structure, bonding and chemical stability of TiB_2, NbB_2 and their ternary alloy $Ti_{0.5}Nb_{0.5}B_2$. Phys B 405(2):540–546. https://doi.org/10.1016/j.physb.2009.09.061

[34] Ju X, Zhang F, Chen Z, Ji G, Wang M, Wu Y, Zhong S, Wang H (2017) Microstructure of multi-pass friction-stir-processed Al–Zn–Mg–Cu alloys reinforced by nano-sized TiB_2 particles and the effect of T6 heat treatment. Metals 7(12):530–544. https://doi.org/10.3390/met7120530

[35] Ma Y, Addad A, Ji G, Zhang M-X, Lefebvre W, Chen Z, Ji V (2020) Atomic-scale investigation of the interface precipitation in a TiB_2 nanoparticles reinforced Al–Zn–Mg–Cu matrix composite. Acta Mater 185:287–299. https://doi.org/10.1016/j.actamat.2019.11.068

[36] Liu J, Chen Z, Zhang F, Ji G, Wang M, Ma Y, Ji V, Zhong S, Wu Y, Wang H (2018) Simultaneously increasing strength and ductility of nanoparticles reinforced Al composites via accumulative orthogonal extrusion process. Mater Res Lett 6(8):406–412. https://doi.org/10.1080/21663831.2018.1471421

[37] De Siqueira RP, Sandim HRZ, Raabe D (2013) Particle stimulated nucleation in coarse-grained ferritic stainless steel. Metall Mater Trans A 44(1):469–478. https://doi.org/10.1007/s11661-012-1408-x

[38] Beck PA, Hu H (1966) The origin of recrystallization textures. In: Margolin H (ed) Recrystallization, grain growth and texture. American Society for Metals, Metals Park, OH, pp 393–433

[39] Ibe G, Lücke K (1966) Growth selection during recrystallization of single crystals. In: Margolin H (ed) Recrystallization, grain growth and textures. ASM, Metals Park, OH, pp 434–447

[40] Clarke A, Humphreys F, Bate PS (2003) Lattice rotations at large second-phase particles in polycrystalline aluminum. Mater Sci Forum 426:399–404. https://doi.org/10.4028/www.scientific.net/MSF.426-432.399

[41] Tang Y, Chen Z, Borbély A, Ji G, Zhong SY, Schryvers D, Ji V, Wang HW (2015) Quantitative study of particle size distribution in an in-situ grown Al–TiB2 composite by synchrotron X-ray diffraction and electron microscopy. Mater Charact 102:131–136. https://doi.org/10.1016/j.matchar.2015.03.003

[42] Huang K, Marthinsen K, Zhao Q, Logé RE (2018) The double-edge effect of second-phase particles on the recrystallization behaviour and associated mechanical properties of metallic materials. Prog Mater Sci 92:284–359. https://doi.org/10.1016/j.pmatsci.2017.10.004

[43] Gottstein G, Molodov DA, Shvindlerman LS (1998) Grain boundary migration in metals: recent developments. Interface Sci 6:7–22. https://doi.org/10.1023/A:1008641617937

[44] Jensen DJ, Hansen N, Humphreys FJ (1985) Texture development during recrystallization of aluminium containing large particles. Acta Metall 33(12):2155–2162. https://doi.org/10.1016/0001-6160(85)90176-2

[45] Huang K, Engler O, Li Y, Marthinsen K (2015) Evolution in microstructure and properties during non-isothermal annealing of a cold-rolled Al–Mn–Fe–Si alloy with different microchemistry states. Mater Sci Eng A 628:216–229. https://doi.org/10.1016/j.msea.2015.01.064

[46] Liu W, Morris J (2007) Recrystallization textures of the M {1 1 3}< 1 1 0> and P {0 1 1}< 4 5 5> orientations in a supersaturated Al–Mn alloy. Scr Mater 56(3):217–220. https://doi.org/10.1016/j.scriptamat.2006.10.011